

## Regular Article

## Discovery of Potent Antiproliferative Agents Targeting EGFR Tyrosine Kinase Based on the Pyrido[3',2':4,5]thieno[3,2-*d*]pyrimidin-4-amine Scaffold

Yasmine Mohamed Abdel Aziz,<sup>a</sup> Mohamed Mokhtar Said,<sup>a</sup> Hosam Ahmed El Shihawy,<sup>a</sup> Mai Fathy Tolba,<sup>b</sup> and Khaled Abouzid Mohamed Abouzid<sup>\*c</sup>

<sup>a</sup>Pharmaceutical Organic Chemistry Department, Faculty of Pharmacy, Suez Canal University; Ismailia 41522, Egypt; <sup>b</sup>Department of Pharmacology and Toxicology, Faculty of Pharmacy, Ain Shams University; Cairo 11566, Egypt; and <sup>c</sup>Pharmaceutical Chemistry Department, Faculty of Pharmacy, Ain Shams University; Cairo 11566, Egypt.

Received July 29, 2015; accepted September 9, 2015

A series of pyridothieno[3,2-*d*]pyrimidin-4-amines was designed and synthesized as congeners to the classical 4-anilinoquinazolines as ATP-competitive epidermal growth factor receptor (EGFR) inhibitors. Compound 5a exhibited the most potent and selective inhibitory activity against EGFR with an IC<sub>50</sub> value of 36.7 nM. Moreover, compounds 4b and 5a showed remarkable cell growth inhibition against leukemia, central nervous system cancer, and non-small cell lung cancer cell lines that overexpress EGFR, with growth inhibition of 50% (GI<sub>50</sub>) values of around 10 nM in the full U.S. National Cancer Institute 60 cell panel assay. Cell cycle studies indicated that compounds 4b and 5a induced significant cell cycle arrest in the S-phase and G0/G1, respectively, in addition to boosting P27<sup>kip</sup> expression. Compound 5a did not alter the viability of placental trophoblasts, which reflects its safety for normal cells. The standard COMPARE analyses demonstrated considerable correlation levels between compounds 4b and 5a and erlotinib, with pyridinium chlorochromate (PCC) values of 0.707 and 0.727, respectively.

**Key words** pyridothieno[3,2-*d*]pyrimidine; epidermal growth factor receptor (EGFR); inhibitor

The epidermal growth factor receptor (EGFR) is a transmembrane receptor tyrosine kinase (RTK) that plays a vital role in signaling pathways that regulate cellular growth, proliferation and survival.<sup>1</sup> Such signaling pathways are triggered by a tightly regulated protein phosphorylation reaction. This reaction is initiated with the binding of the epidermal growth factor (EGF) to the extracellular domain of EGFR leading to the activation of its intrinsic kinase domain. The latter has the ability to activate proteins by removing phosphate groups from ATP and covalently binding them to tyrosine substrates of the proteins.<sup>2</sup> Deregulation of this controlled pathway, through overexpression and/or mutation of EGFR, contributes to the malignant transformations of normal cells. Overexpression of EGFR has been observed in a large number of human cancers including breast, prostate, ovarian, colorectal, kidney, brain and non-small cell lung cancers.<sup>3,4</sup>

Examples of clinically approved ATP-competitive EGFR inhibitors including gefitinib, lapatinib and erlotinib, are structurally based on a central 4-anilinoquinazoline scaffold<sup>5</sup> (Fig. 1). However the emerging resistance of cancer cells to current medicines derives our passion to search for novel congeners to the 4-anilinoquinazoline scaffold as a beached for cancer therapy.<sup>6,7</sup> Structure–activity relationship studies of 4-anilinoquinazolinederivatives revealed that the quinazoline core fits into the ATP-competitive pocket of EGFR.<sup>8,9</sup> Consistent with this, some investigations showed that the isosteric replacement of the benzene ring of the quinazoline core with five-membered heteroaromatic rings is favorable.<sup>10,11</sup> The flexibility of the linking NH group between the heteroaryl core and the aniline ring permits the proper orientation of the aniline ring into the hydrophobic pocket, lying in the back of

the ATP-binding site.<sup>1</sup> This hydrophobic pocket, often called “specificity pocket,” is characteristic for each type of kinases, allowing for the design of selective ligands.<sup>12</sup> On the other side, the substituents present at positions 6 and 7 of the quinazoline core structure, often called “solubilizing tails,” protrude from the ATP-binding site into the solvent.<sup>1,4,11</sup> In this context, Showalter *et al.* reported that fusing a third ring to 6- and 7-positions of the quinazoline ring enhanced the kinase inhibitory activity over the parent bicyclic analogues.<sup>11</sup>

On the other hand, the discovery of potent inhibitors of a particular kinase often commence with the screening of the archived inhibitors that were studied in previous reports. Thus, the analogue synthesis approach is generally initiated with a lead scaffold that was first identified as a promising inhibitor for a certain kinase then modified to inhibit another member of the kinase family.<sup>12</sup> Based on this, the pyridothienopyrimidine scaffold reported by Loidreau *et al.* as promising CK1 and CLK1 kinases inhibitors could be considered as one of the lead scaffolds that could be modified to provide novel EGFR inhibitors.<sup>13</sup>

In a completion of our previous work on the pyridothieno[3,2-*d*]pyrimidine analogues that have been discovered as promising vascular endothelial growth factor receptor (VEGFR)-2 inhibitors,<sup>14</sup> we initiated this study with the aim of expanding the efficiency of the pyridothieno[3,2-*d*]pyrimidine scaffold as ATP-competitive EGFR inhibitors. Our strategy is directed toward the design of a focused library of novel pyridothieno[3,2-*d*]pyrimidine analogues on the basis of 3 main modifications. We envisioned that the potency and the selectivity of these analogues might be enhanced by modifying the length of NH spacer and/or by varying the aniline sub-

\* To whom correspondence should be addressed. e-mail: Khaled.abouzid@pharma.asu.edu.eg

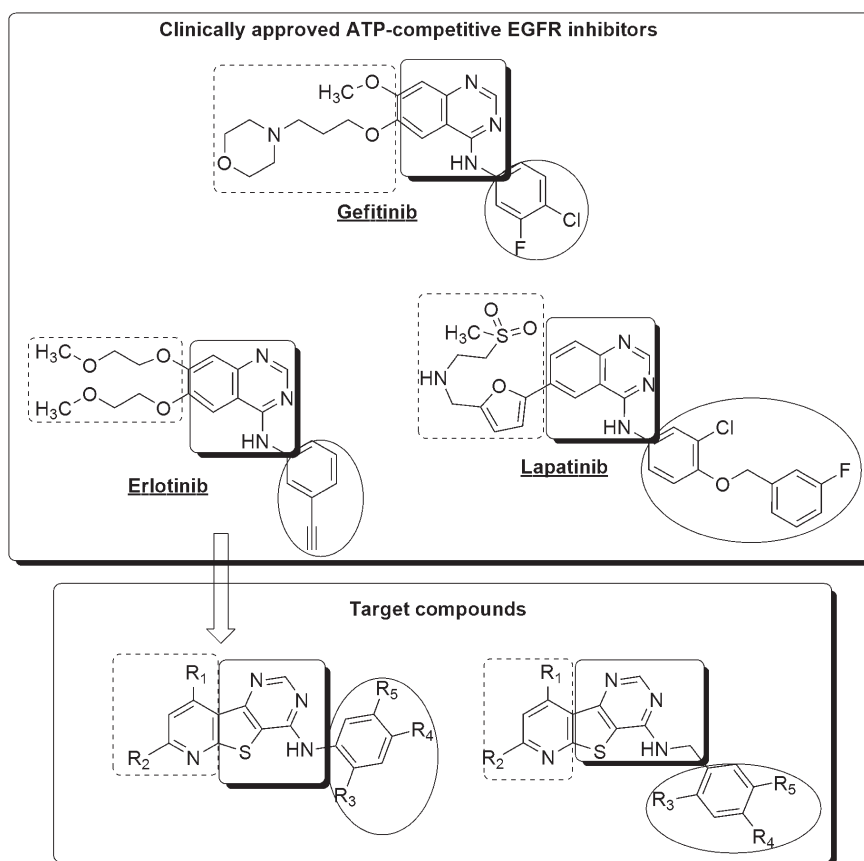
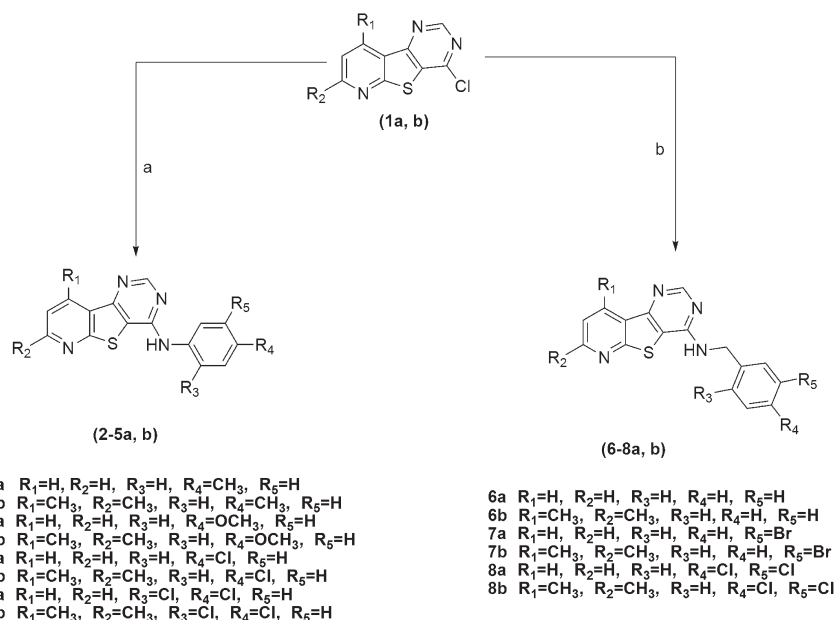


Fig. 1. The Design of the Targeted Compounds as ATP-Competitive EGFR Inhibitors

The key structural elements used in the design of the targeted compounds are highlighted as follows: (the heteroaryl core and the linking group=shadowed rectangle); (the solubilizing moiety=dashed rectangle) and (the hydrophobic aryl moiety=solid circle).



Reagents and conditions: (a) Aniline derivatives, dry THF, Et<sub>3</sub>N, reflux, 18–20h; (b) Benzylamine derivatives, dry DCM, Et<sub>3</sub>N, reflux 6–9h.

Chart 1. Synthesis of Targeted Compounds (2–8a, b)

stitution pattern. In addition, the variation of the substitution pattern on the third pyridine ring and the exploitation of the basic pyridine nitrogen to act as a solubilizing moiety (Fig. 1).

## Results and Discussion

**Chemistry** The 4-chloropyrido[3',2':4,5]thieno[3,2-*d*]pyrimidine derivatives (**1a, b**) have been prepared as reported earlier by our group.<sup>14</sup> Compounds (**1a, b**) have been allowed to react with a variety of substituted anilines and benzyl-

amines respectively to afford the target compounds (**2–8a, b**) (Chart 1).

The structures of the targeted compounds (**2–8a, b**) were established on the basis of their elemental analyses and spectral data (MS, IR, <sup>1</sup>H-NMR and <sup>13</sup>C-NMR). The <sup>1</sup>H-NMR spectra of the target compounds (**2–5a, b**) displayed characteristic aromatic protons, which were assigned to the aniline ring, in the range of 6.37–8.38 ppm. The <sup>1</sup>H-NMR spectra of compounds (**3a, b**) were characterized by the appearance of a singlet peak at 3.99–4.20 ppm characteristic for OCH<sub>3</sub> protons. In the <sup>1</sup>H-NMR spectra of the targeted compounds (**6–8a, b**), a characteristic singlet peak corresponding to the benzylic protons have been displayed at 3.97–4.91 ppm. The <sup>1</sup>H-NMR spectra were characterized also by the appearance of multiplet signals corresponding to the benzyl ring at 7.19–7.75 ppm. The IR spectra showed collectively secondary amine signals in the range of 3300–3500 cm<sup>-1</sup> that indicated the successful coupling of 4-chloropyrido[3',2':4,5]thieno[3,2-*d*]pyrimidine derivatives (**1a, b**) with the aromatic amines. Moreover, the <sup>13</sup>C-NMR and mass spectra of the target compounds are in agreement with the proposed structures.

### Biological Evaluation

#### Protein Kinase Inhibitory Assays

##### The Initial Screening Assay

The protein kinase inhibitory assays were performed at BPS Bioscience laboratories.<sup>15)</sup> In the initial screening assay, compounds (**3b**) and (**4–6a, b**) were tested at a single concentration 10 μM over a panel of six human kinases. VEGFR-1/Flt-1 (BPS #40223), VEGFR-2/KDR (BPS #40301) and the wild type of EGFR (BPS #40187) are tyrosine kinases. Cyclin-dependent kinase (CDK)5/p25 (BPS #40105), GSK3α (BPS #40006) and GSK3β (BPS #40007) are serine/threonine kinases.

Compound (**5a**) exhibited kinase inhibitory activity against EGFR with 81% percentage of inhibition at 10 μM and IC<sub>50</sub>%. While compound (**4b**) inhibited EGFR at 10 μM with 70% percentage of inhibition. The percentages of EGFR inhibition exerted by the other tested compounds were below 60%<sup>16)</sup> (Table 1).

Structure–activity relationship (SAR) studies for the ability of pyridothienopyrimidine scaffold to inhibit EGFR-TKs activity revealed that both of the pyrimidine nitrogen atoms were absolutely essential for activity. Furthermore, the fusion of a third ring containing basic nitrogen such as the pyridine ring might enhance the physical properties of the tricyclic core structure. The substitution on the pyridine ring was confined to small alkyl substituents such as methyl group. In general, compounds with halogenated aniline moiety displayed higher

activity than non-halogenated as it might be able to occupy the lipophilic regions in the ATP binding site of EGFR-TK. The nature of the linking group between the tricyclic core structure and phenyl side chain has a great effect on the inhibitory activity. Upon increasing the length of this spacer by one carbon atom **6a, b–8a, b**, we noticed a reduction in the anticancer activity.

In the rigid tricyclic ring system, combination of dimethyl groups on pyridine ring with dichloro substituents on the aniline ring might hinder optimum binding of the compound **5b** into the ATP binding site of EGFR leading to lesser inhibitory activity than that with unsubstituted pyridine ring with dichloro aniline **5a**. On the other hand, compound **4b** with only one chloro substituent at the 4-position on the anilino moiety and dimethyl groups on the pyridine ring of the tricyclic scaffold compound of **4b** could lead to optimum binding.

#### Measurement of Potential Enzyme Inhibitory Activity IC<sub>50</sub>

The profiling data for compound (**5a**) against EGFR showed an IC<sub>50</sub> value 36.7 nM. This IC<sub>50</sub> value of compound (**5a**) is superior to the one exerted by the standard anti-EGFR erlotinib against the wild type of EGFR, which is 486 nM (Table 1).<sup>17)</sup>

#### *In Vitro* Anticancer Screening

The newly synthesized compounds were submitted to National Cancer Institute NCI, Bethesda, Maryland, U.S.A., under the Developmental Therapeutic Program DTP.<sup>18)</sup> The operation of this screening utilized 60 different human cancer cell lines, including leukemia, melanoma, lung, colon, brain, ovary, breast, prostate and kidney cancers. Compounds with drug-like properties are prioritized by the NCI screening service, based on computer-aided design. Six compounds were selected for the primary anticancer screening based on their ability to add diversity to the NCI small molecule compounds collection. The target compounds (**4–6a, b**) were assigned with the following NCI codes NSC D-778769/1, NSC D-776678/1, NSC D-778770/1, NSC D-778771/1, NSC D-774742/1 and NSC D-774743/1, respectively.<sup>18)</sup>

Primary Single High Dose (10<sup>-5</sup> M) against Full NCI 60 Cells Panel *in Vitro* Assay

Primary *in vitro* one dose anticancer screening was performed utilizing the full NCI 60 cell lines' panel. Results for each compound were reported as a mean graph of the percent growth of the treated cells when compared to the untreated control cells. The percentage growth of the target compounds (**4–6a, b**) against the full 60-cell line panel are illustrated in (Table S1). After obtaining the results for the single dose assay, an analysis of the historical Development Therapeutics Program (DTP) was performed and compounds (**4b**) (NSC D-776678/1) and (**5a**) (NSC D-778770/1) which satisfied the predetermined threshold inhibition criteria were selected for the NCI full panel 5 doses assay (Figs. 2, 3).

#### *In Vitro* 5 Doses Full NCI 60 Cell Panel Assay

All the 60 cell lines, representing nine cancer subpanels, were incubated at five different concentrations (0.01, 0.1, 1, 10 and 100 μM) of the tested compounds. The outcomes were used to create log<sub>10</sub> concentration *versus* percentage growth inhibition curves and three response parameters (GI<sub>50</sub>, total growth inhibition (TGI) and LC<sub>50</sub>) were calculated for each cell line. The GI<sub>50</sub> value (growth inhibitory activity) corresponds to the concentration of the compound causing 50% decrease in net cell growth. The TGI value (cytostatic activity) is the concentration of the compound resulting in total growth

Table 1. Summary of the % Inhibitory Effects of Targeted Compounds (**3b**) and (**4–6a, b**) on EGFR Activity

Compound	EGFR	IC <sub>50</sub> (nM)
<b>3b</b>	52 <sup>a)</sup>	—
<b>4a</b>	48	—
<b>4b</b>	70	—
<b>5a</b>	81	36.7
<b>5b</b>	55	—
<b>6a</b>	26	—
<b>6b</b>	33	—
Erlotinib	—	486

a) % Inhibition values of compounds on EGFR activity at 10 μM.

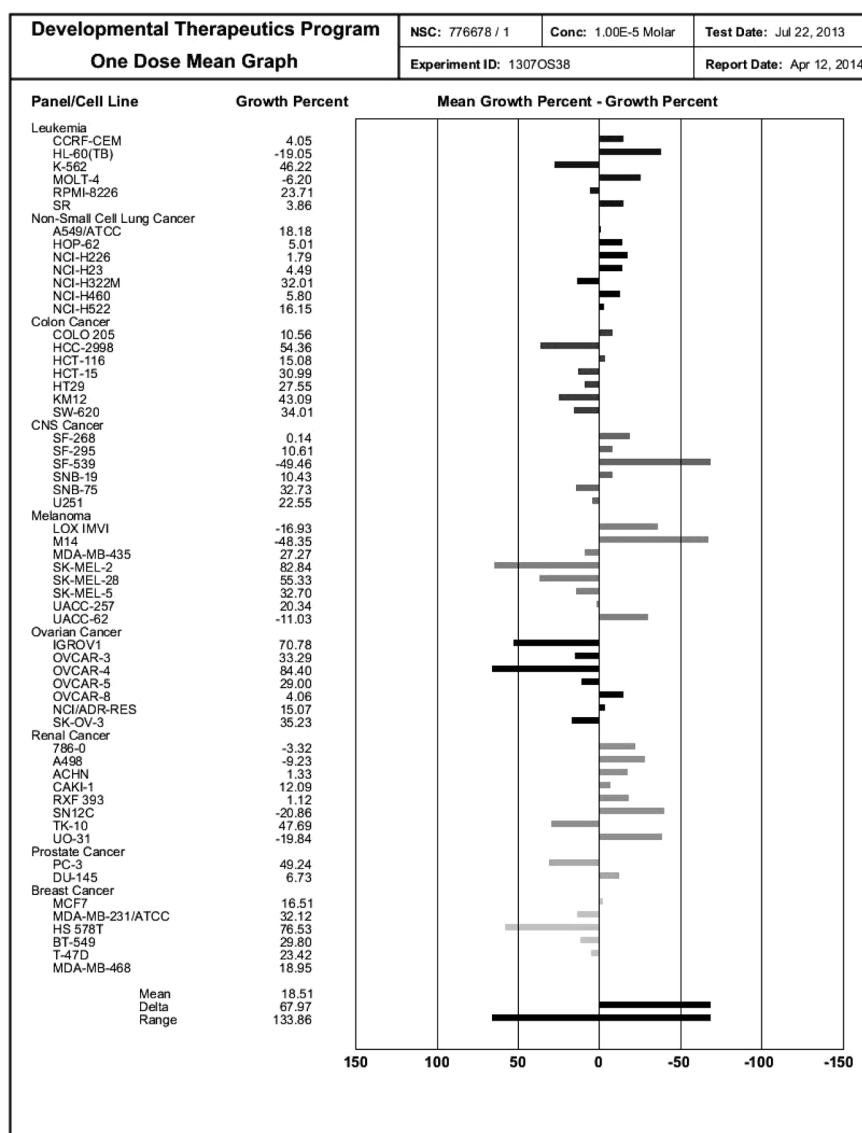


Fig. 2. One Dose Mean Graph of Compound (**4b**)

Nine panels were tested and color coded.

inhibition. The  $LC_{50}$  value (cytotoxic activity) is the concentration of the compound causing net 50% loss of initial cells at the end of the incubation period of 48 h.

Compounds (**4b**) and (**5a**) showed a distinctive pattern of selectivity and sensitivity against different NCI cell panels regarding to sensitivity against individual cell lines, as illustrated in (Table S2), respectively. Collective dose response curves and individual dose response curves of all cell lines tested for compounds (**4b**) and (**5a**) were shown in Figs. 4–7, respectively. Compound (**4b**) (NSC D-776678/1) exhibited a remarkable anticancer activity against most of the tested cell lines representing nine different subpanels with  $GI_{50}$  values between “10–85 nM,” except eleven cell lines namely NCI-H322M, HCC-2998, KM12, MALME-3M, SK-MEL-2, SK-MEL-28, IGROV1, OVCAR-3, OVCAR-4, TK-10 and HS 578T showed  $GI_{50}$  values  $>100$  nM (Figs. 4, 5). The obtained data revealed an obvious sensitivity profile toward leukemia subpanel ( $GI_{50}$  value ranging from  $<10$  to 19.70 nM), least for CCRF-CEM, HL-60(TB), MOLT-4, SR cell lines and maximum for RPMI-8226 cell line. Central nervous system (CNS) cancer

subpanel also showed higher sensitivity ( $GI_{50}$  value ranging from  $<10$  to 28.70 nM), least for SF-268, SF-539, SNB-19U251 and maximum for SF-295 (Table S2).

Compound (**5a**) (NSC D-778770/1) exhibited a remarkable anticancer activity against most of the tested cell lines representing nine different subpanels with  $GI_{50}$  values between “10–98 nM,” except fifteen cell lines namely K-562, NCI-H322M, COLO 205, HCC-2998, KM12, SNB-75, SK-MEL-2, SK-MEL-28, IGROV1, OVCAR-3, OVCAR-4, SN12C, TK-10, MDA-MB-231/ATCC and HS 578T showed  $GI_{50}$  values  $>100$  nM (Figs. 6, 7). The obtained data revealed an obvious sensitivity profile toward NSCLC subpanel ( $GI_{50}$  value ranging from  $<10$  to 100 nM), least for A549/ATCC, HOP62, NCI-H23, NCI-H460 cell lines and maximum for NCI-H322M cell line (Table S2).

The criterion for selectivity of a compound depends upon the ratio obtained by dividing the full panel MID (the average sensitivity of all cell lines toward the test agent) by their individual subpanel MID (the average sensitivity of all cell lines of a particular subpanel toward the test agent). As per

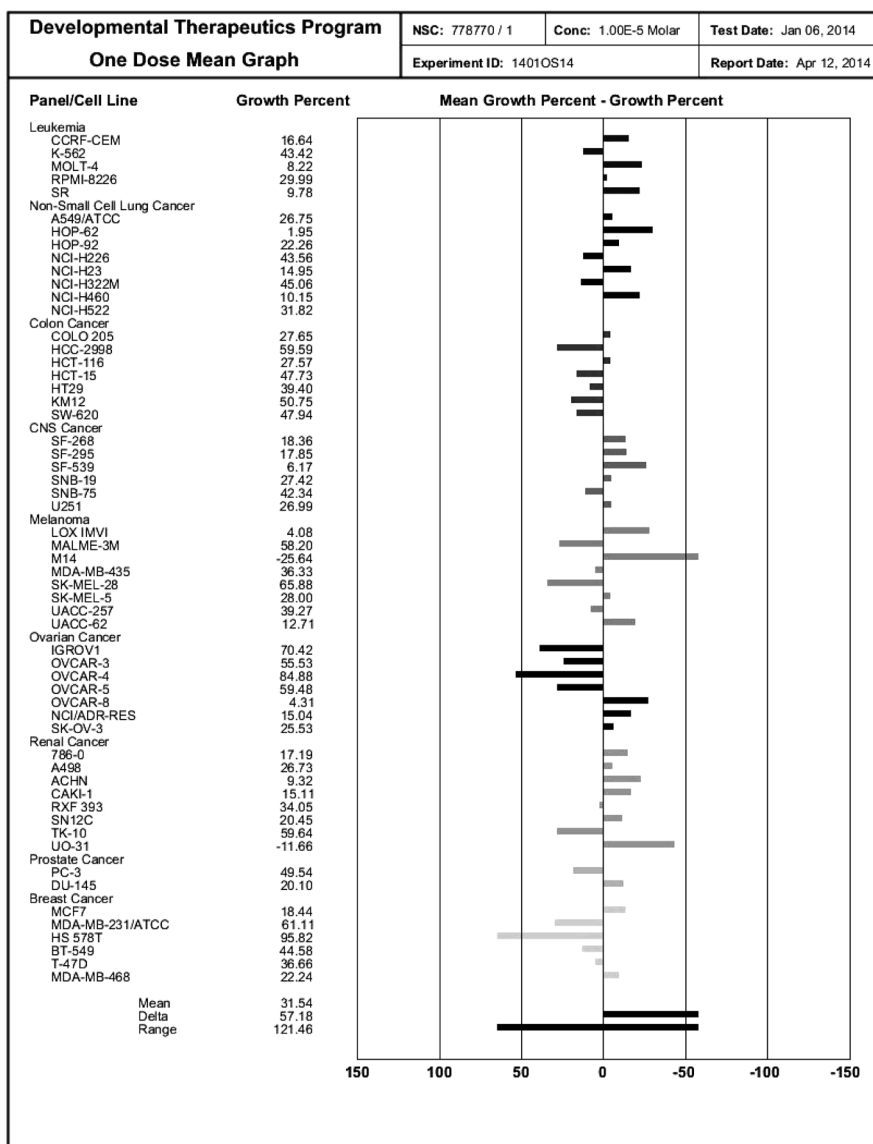


Fig. 3. One Dose Mean Graph of Compound (**5a**)

Nine panels were tested and color coded.

this criterion, compound (**4b**) was found to be most selective toward leukemia and CNS cancer subpanels, with selectivity ratios 2.69 and 2.40, respectively. While compound (**5a**) was found selective toward CNS cancer, leukaemia and NSCLC subpanels with selectivity ratios 1.40, 1.17 and 1.16, respectively. It is well known that EGFR is highly expressed in cell lines derived from CNS cancer and NSCLC.<sup>19,20)</sup>

#### COMPARE Analyses

COMPARE analyses were performed for compounds (**4b**) and (**5a**) in order to investigate the similarity of their cytotoxicity patterns with those of the standard anticancer agents, in the NCI database.<sup>21)</sup> Such analyses are based on comparing the patterns of the differential growth inhibition of the tested compounds against the cultured cancer cell lines. Thus, we can potentially gain insight into the mechanism of their growth inhibitory effects. When the growth inhibition pattern of certain compound correlates well with that of a standard agent, the Pearson's correlation coefficient value will be greater than 0.6 (PCC >0.6). Consequently, the compound of interest might acquire the same mechanism of action.<sup>21)</sup>

The standard COMPARE analyses are performed at the  $GI_{50}$  levels. that the results of COMPARE analyses indicated that compounds (**4b**) and (**5a**) demonstrate considerable correlation levels with erlotinib (NSC 718781) with PCC values 0.707 and 0.727, respectively. Such similarity in the COMPARE results could indicate a potential resemblance in the mechanism of action of compounds (**4b**) and (**5a**) with erlotinib, which is a potent ATP-competitive EGFR inhibitor.<sup>1,4)</sup>

In the light of the NCI results, the following considerations could be made. The anticancer activities of compounds (**4–6a, b**) were sensitive to the length of the NH spacer between the tricyclic core and the phenyl ring. This could be observed in the anticancer profiles of compounds (**4, 5a, b**) when compared to compounds (**6a, b**). The increase in the length of the NH spacer by one carbon atom led to a significant decrease in the anticancer activity. Furthermore, compounds (**4b**) and (**5a**) were the most active members among the synthesized series with mean percentage growth values of 18.51 and 31.54%, respectively. Compounds (**4b**) and (**5a**) were selective toward leukaemia, CNS cancer and NSCLC cell lines, in the 5 doses

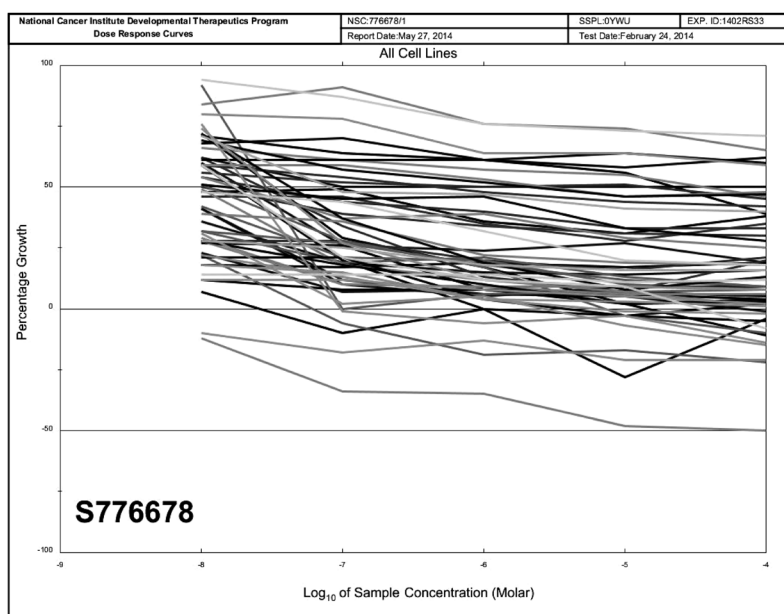


Fig. 4. Collective Dose Response Curves of Compound (4b) for All NCI 60 Cell Lines of *in Vitro* 5 Dose Assay

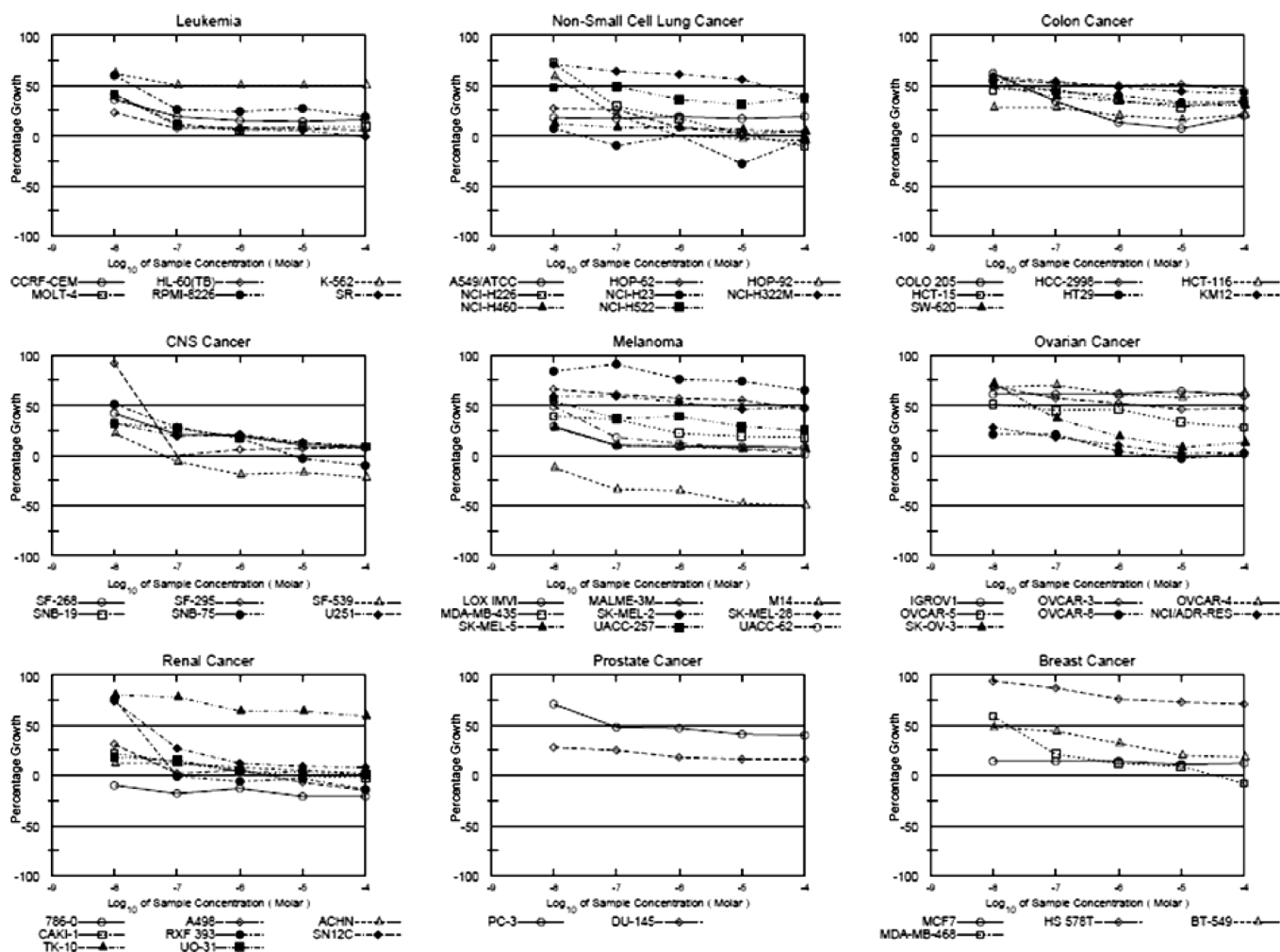


Fig. 5. Individual Dose Response Curves of Compound (4b) for All NCI 60 Cell Line

full NCI 60 cell panel assay. COMPARE analyses illustrated a high correlation between  $GI_{50}$  mean graphs of compounds (4b), (5a) and the standard ATP-competitive EGFR inhibitor

erlotinib with PCC values 0.707 and 0.727, respectively. Moreover, compound (5a) inhibited EGFR selectively with  $IC_{50}$  value 36.7 nM when it was tested over a panel of six kinases.

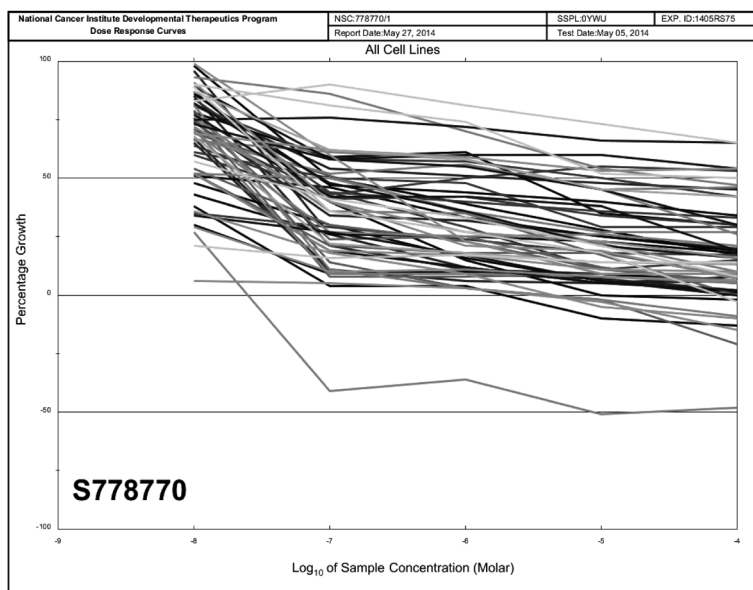


Fig. 6. Collective Dose Response Curves of Compound (5a) for All NCI 60 Cell Lines of *in Vitro* 5 Dose Assay

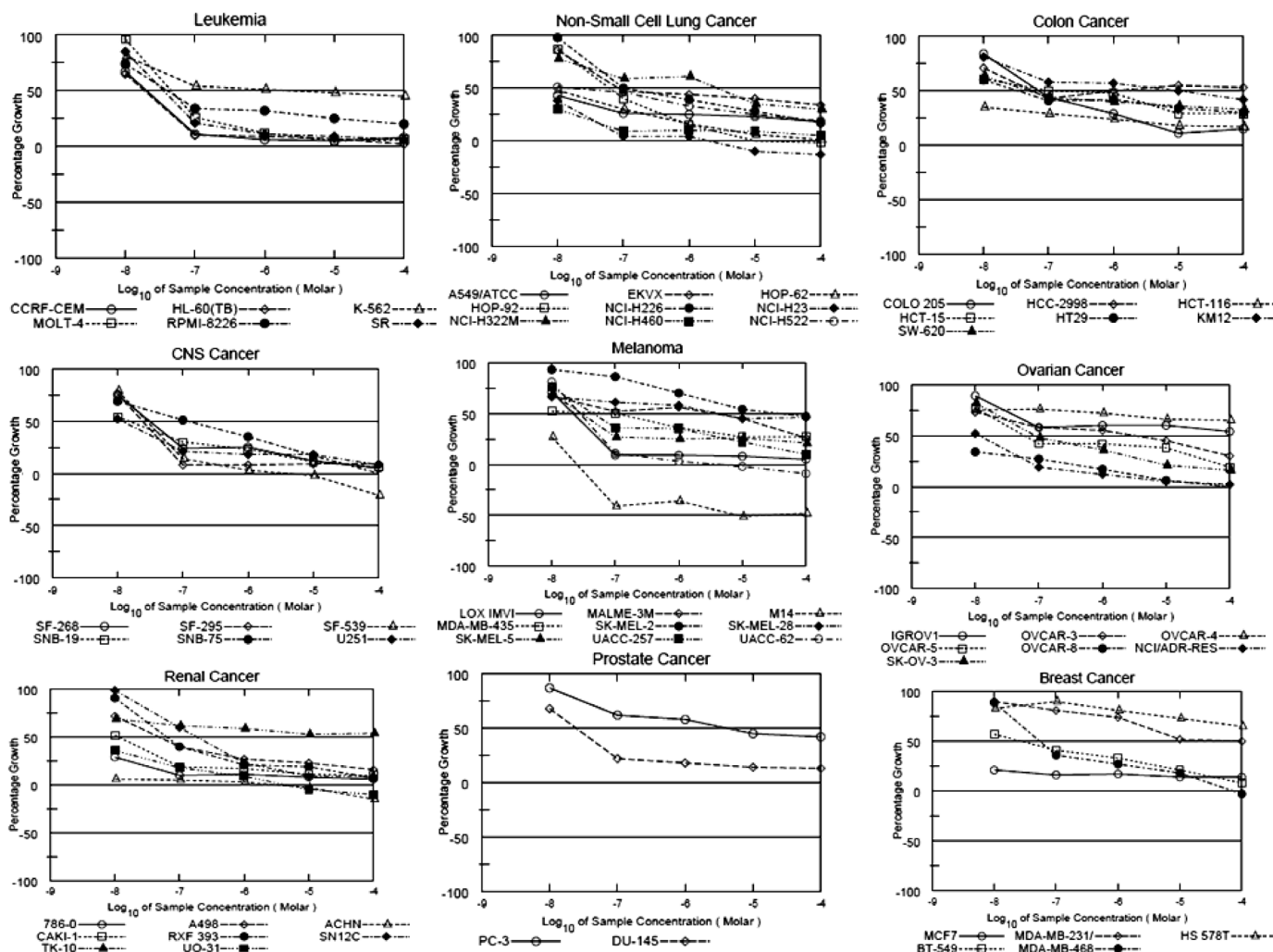


Fig. 7. Individual Dose Response Curves of Compound (5a) for All NCI 60 Cell Lines

These results might support our strategy of designing ATP-competitive EGFR inhibitors as anticancer agents.

**Cell Cycle Studies**

IC<sub>50</sub> Using Sulforhodamine B (SRB) Assay

The cytotoxicity of compounds (4b) and (5a) against A549

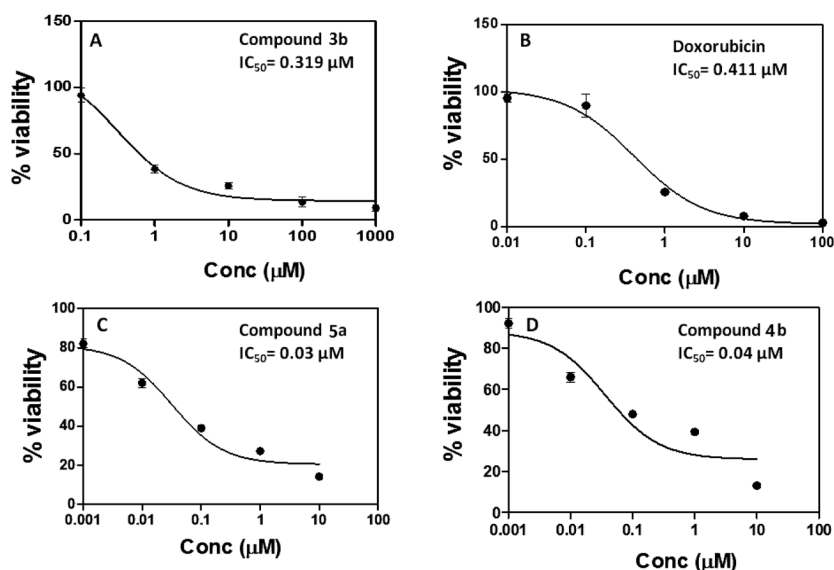


Fig. 8. Concentration–Response Curves of Compounds (**3b**, **4b**, **5a**) Compared to Doxorubicin in A549 Human Lung Cancer Cells

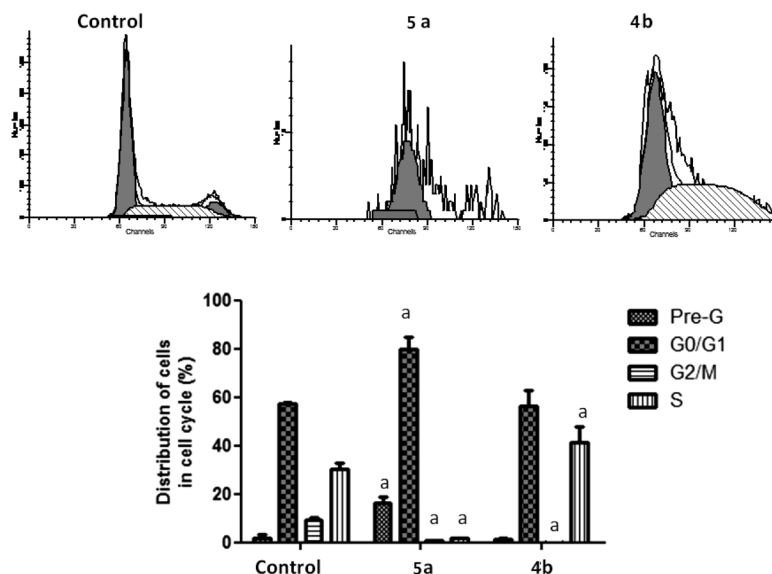


Fig. 9. Effect of Compounds (**4b**) and (**5a**) on DNA-Ploidy Flow Cytometric Analysis of A549 Cells

The cells were treated with compounds (**4b**) or (**5a**) at their  $IC_{50}$  (0.04, 0.03  $\mu M$ ) for 48 h. Data are mean  $\pm$  S.D. ( $n=3$ ). Experiments were done in triplicate.

human non-small cell lung cancer cell line was tested using SRB assay and the  $IC_{50}$  values were 0.04 and 0.03  $\mu M$ , respectively (Fig. 8).

#### Effects of Compounds (**4b**) and (**5a**) on the Cell Cycle

DNA-flow cytometry was conducted in order to investigate the effects of the tested compounds on the cell cycle. Exposure of A549 lung cancer cells to compounds (**4b**) and (**5a**) at a concentration equal to their  $IC_{50}$  for 48 h induced marked changes in the cell cycle. Exposure to compound (**5a**) produced significant increase in cell death as evidenced from increased accumulation of cells at Pre-G phase by 8.5 folds ( $p<0.001$ ) compared to control. It also induced significant increase in the percentage of cells at G0/G1 phase by 1.4 folds ( $p<0.01$ ) indicating arrest at this phase with subsequent reduction in the percentage of cells at G2/M and S-phases by about 88.7 ( $p<0.001$ ) and 93% ( $p<0.001$ ), respectively compared to control (Fig. 9). On the other hand, treatment of A549 cells

with compound (**4b**) induced significant increase in the cells accumulated at S-phase by about 1.4 folds ( $p<0.001$ ) with subsequent reduction in the percentage of cells at G2/M phase by about 98% ( $p<0.05$ ) compared to control. Erlotinib was previously reported to induce cell cycle arrest at G0/G1 in NSCLC cells.<sup>22,23</sup> The pattern of cell cycle arrest induced by compound (**5a**) is more close to that previously reported for erlotinib in NSCLC and this further support the results from COMPARE analysis.

#### Effects of Compounds (**4b**) and (**5a**) on the Expression of P27<sup>kip</sup>

The significant cell cycle arrest induced by compounds (**4b**) and (**5a**) in A549 cell line was further substantiated through assessing the expression levels of the cell cycle inhibitory protein P27<sup>kip</sup>. It is a member of the Cip/Kip family of cyclin-dependent kinase inhibitors. This family functions through the formation of heterotrimeric complexes with cyclins and

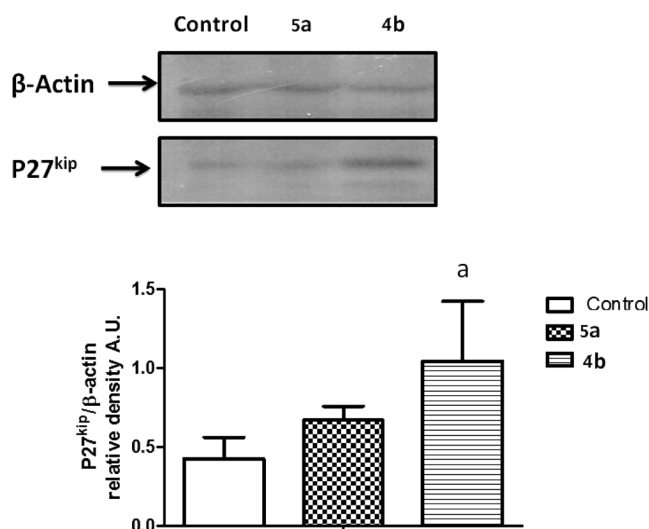


Fig. 10. The Effect of Compounds (**4b**) and (**5a**) on the Protein Expression of p27<sup>kip</sup> in A549 Cells as Assessed through Western Blotting

Data are mean  $\pm$ S.D. ( $n=3$ ). Experiments were done in triplicate.

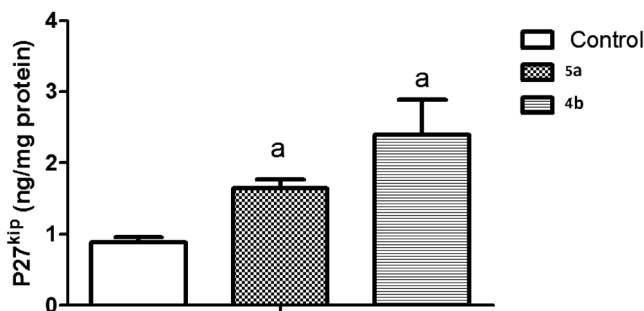


Fig. 11. The Effect of Compounds (**4b**) and (**5a**) on the Protein Expression of p27<sup>kip</sup> in A549 Cells as Assessed through ELISA

Data are mean  $\pm$ S.D. ( $n=3$ ). Experiments were done in triplicate.

cyclin-dependent kinases (CDKs) leading to abolishing kinase activity and block of cell cycle progression through G1/S phase.<sup>24</sup> The expression levels of p27 are down-regulated in different human cancers and are associated with poor prognosis.<sup>25</sup> Treatment of the cells with compounds (**5a**) and (**4b**) triggered induction in the protein expression of P27<sup>kip</sup> by about 2.5 and 1.6 ( $p<0.05$ ) folds compared to control as indicated by Western blotting (Fig. 10). Assessment of P27<sup>kip</sup> levels using enzyme-linked immunosorbent assay (ELISA) further supported the changes observed with Western blotting with significant increase in P27<sup>kip</sup> levels by about 2.7 ( $p<0.05$ ) and 1.7 ( $p<0.01$ ) folds respectively after treatment with compounds (**4b**) and (**5a**) compared to untreated cells (Fig. 11). Downregulation of EGFR was reported to be related to the induction of P27<sup>kip</sup> expression *in vitro* and in human tumor specimens.<sup>26</sup> Compounds (**4b**) and (**5a**) showed strong inhibition for EGFR enzyme activity *in vitro* by about 70 and 81%. This might at least partly explain their ability to induce the expression of p27<sup>kip</sup>. Erlotinib-induced G0/G1 arrest and cell growth inhibition was linked to its ability to induce P27<sup>kip</sup> expression in NSCLC cells. Therefore, cell cycle arrest induced by the tested compounds is at least partly attributed to the ability of the tested compounds to boost the expression of P27<sup>kip</sup>.

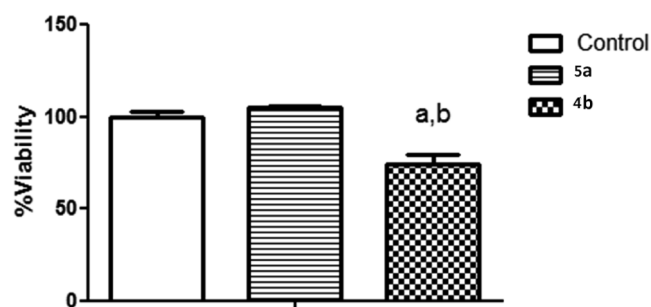


Fig. 12. Effect of the IC<sub>50</sub> of Compounds (**4b**) and (**5a**) on the Viability of Normal Placental Cytotrophoblasts

Data are mean  $\pm$ S.D. ( $n=3$ ). Experiments were done in triplicate.

Table 2. Cytotoxic Activities of Compounds (**2–3a, b**) and (**7–8a, b**)

Compound	IC <sub>50</sub> values (in $\mu\text{M}$ ) <sup>a)</sup>	
	A549	MCF7
<b>2a</b>	2.75	307.7
<b>2b</b>	3.43	42.61
<b>3a</b>	0.359	10.71
<b>3b</b>	0.319	7.32
<b>7a</b>	339.1	266.5
<b>7b</b>	1061	841.9
<b>8a</b>	567.9	266.7
<b>8b</b>	233.1	113.4
Doxorubicin	0.411	1.172

a) IC<sub>50</sub> is defined as the concentration which results in a 50% decrease in cell number as compared with that of the control cultures in the absence of an inhibitor. The values represent the mean  $\pm$ S.E. of three individual observations.

#### Effect of the Tested Compounds (**4b**) and (**5a**) on the Viability of Normal Cells

Exposure of villous cytotrophoblast placental cell line to compounds (**5a**) and (**4b**) for 72 h (These concentrations are equivalent to their IC<sub>50</sub> in A549 lung cancer cells.) produced a significant reduction in the cell viability after exposure to compound (**4b**) by about 25% ( $p<0.001$ ) compared to control and compound (**5a**). It is noteworthy that the viability of the normal cells was preserved after treatment with compound (**5a**) (Fig. 12).

#### SRB Cytotoxicity Assay

Compounds (**2, 3a, b**) and (**7, 8a, b**) that were not selected by NCI screening service, were tested for cytotoxicity against 2 human cancer cell lines, namely A549-lung cancer and MCF7-breast cancer, using sulforhodamine B (SRB) assay as described by Skehan *et al.* Doxorubicin was used as a reference standard.<sup>27</sup> The IC<sub>50</sub> values of the test compounds were presented in (Table 2). Compounds (**3a**) and (**3b**) showed promising activities with IC<sub>50</sub> values  $<1\ \mu\text{M}$  against A549-lung cancer cell line, while compounds (**2a**) and (**6b**) showed moderate activities with IC<sub>50</sub> values  $<10\ \mu\text{M}$ . The high activities of compounds (**7a**) and (**7b**) could be attributed to the presence of methoxy group at position 4 of the aniline ring, whereas the presence of benzylic CH<sub>2</sub> linker dramatically reduced the activities of compounds (**7, 8a, b**). The previous findings highlighted compound (**3b**) as potential anti-proliferative agent with IC<sub>50</sub> value  $0.319\ \mu\text{M}$  superior to that of the standard doxorubicin  $0.411\ \mu\text{M}$  against A549-lung cancer cell line (Fig. 8). However, compounds (**5a**) and (**4b**) are still the ones showing

the highest potency against A549 among the tested series with IC<sub>50</sub> values of 0.03 and 0.04 μM, respectively.

## Experimental

**Chemistry** The structures of all tested compounds were confirmed by <sup>1</sup>H-NMR, <sup>13</sup>C-NMR and mass spectrometry (electron ionization (EI)-MS). The purities of the tested compounds were determined by elemental analysis. The commercial chemicals and solvents were reagent grade and used without further purification. <sup>1</sup>H- and <sup>13</sup>C-NMR spectra were measured in DMSO-*d*<sub>6</sub> on a Varian Mercury VX-300 NMR spectrometer or Jeol LA (400 MHz for <sup>1</sup>H-NMR, 100 MHz for <sup>13</sup>C-NMR). Chemical shifts were reported in parts per million (ppm) using tetramethylsilane (TMS) as an internal standard. Electron impact mass spectra were recorded on Shimadzu GCMS-QP 5050 A gas chromatograph mass spectrometer (70 eV). Elemental analysis was performed at the Microanalytical Center of Cairo University, Egypt. IR spectra were recorded on a Shimadzu FT-IR 8101 PC IR spectrophotometer (KBr pellets). Values were represented in cm<sup>-1</sup>. The synthetic procedure for the compounds was illustrated in (Chart 1).

### General Procedures for the Synthesis of *N*-(Substituted Phenyl)pyrido[3',2':4,5]thieno[3,2-*d*]pyrimidin-4-amines (2–5a, b)

The appropriate aniline (9 mmol) was dissolved in dry tetrahydrofuran (THF) (25 mL) and Et<sub>3</sub>N (1.5 mL) under nitrogen atmosphere. Compound (1a or b) (4.5 mmol) was added slowly to the stirred solution which was then heated under reflux for 15–20 h. The reaction mixture was cooled and poured onto crushed ice. The precipitated solid was filtered off, washed with water (2×10 mL) and dried. The crude solid was purified by column chromatography using 1–2 EtOAc/hexane v/v as the eluent to give the desired compounds (2–5a, b).

#### *N*-(4-Tolyl)pyrido[3',2':4,5]thieno[3,2-*d*]pyrimidin-4-amine (2a)

Yield 53%; mp 276–278°C. <sup>1</sup>H-NMR (DMSO-*d*<sub>6</sub>) δ: 11.07 (1H, s), 8.71 (1H, dd, <sup>3</sup>J=4.80 Hz, <sup>4</sup>J=2.00 Hz), 7.93 (1H, d, <sup>3</sup>J=8.00 Hz), 7.44 (1H, s), 7.16 (1H, t, <sup>3</sup>J=8.00 Hz); 6.71 (4H, dd, <sup>3</sup>J=8.4 Hz, <sup>4</sup>J=1.2 Hz), 2.30 (3H, s). IR (KBr) cm<sup>-1</sup>: 3427, 2988, 1621, 1561. MS *m/z*: 294.00 (M<sup>+</sup>+2), 203.00. *Anal.* Calcd for C<sub>16</sub>H<sub>12</sub>N<sub>4</sub>S: C, 65.73; H, 4.14; N, 19.16. Found; C, 66.13; H, 4.54; N, 19.56.

#### *N*-(4-Tolyl)-7,9-dimethylpyrido[3',2':4,5]thieno[3,2-*d*]pyrimidin-4-amine (2b)

Yield 58%; mp 300°C. <sup>1</sup>H-NMR (DMSO-*d*<sub>6</sub>) δ: 10.99 (1H, s), 8.38 (1H, s), 7.82 (1H, s), 7.65 (2H, d, <sup>3</sup>J=9.00 Hz, H-16), 7.23 (2H, d, <sup>3</sup>J=9.00 Hz), 2.24 (6H, s), 1.98 (3H, s). IR (KBr) cm<sup>-1</sup>: 3440, 3033, 2832, 1662, 1570. MS *m/z*: 322.00 (M<sup>+</sup>+2), 231.00. *Anal.* Calcd for C<sub>18</sub>H<sub>16</sub>N<sub>4</sub>S: C, 67.47; H, 5.03; N, 17.49. Found; C, 67.67; H, 5.38; N, 17.60.

#### *N*-(4-Methoxyphenyl)pyrido[3',2':4,5]thieno[3,2-*d*]pyrimidin-4-amine (3a)

Yield 60%; mp > 300°C (decomp.). <sup>1</sup>H-NMR (DMSO-*d*<sub>6</sub>) δ: 9.89 (1H, s), 8.88 (1H, dd, <sup>3</sup>J=5.00 Hz, <sup>4</sup>J=2.00 Hz), 8.60 (1H, d, <sup>3</sup>J=8.00 Hz), 7.99 (1H, s), 7.41 (1H, t, <sup>3</sup>J=8.00 Hz), 6.46 (2H, dd, <sup>3</sup>J=8.00 Hz, <sup>4</sup>J=1 Hz), 6.37 (2H, dd, <sup>3</sup>J=8.00 Hz, <sup>4</sup>J=1 Hz), 4.20 (3H, s). IR (KBr) cm<sup>-1</sup>: 3395, 2907, 1643, 1461. MS *m/z*: 308.00 (M<sup>+</sup>), 203.00. *Anal.* Calcd for C<sub>16</sub>H<sub>12</sub>N<sub>4</sub>OS: C, 62.32; H, 3.92; N, 18.17. Found; C, 61.93; H, 3.70; N, 17.98.

#### *N*-(4-Methoxyphenyl)-7,9-dimethylpyrido[3',2':4,5]thieno[3,2-*d*]pyrimidin-4-amine (3b)

Yield 65%; mp > 300°C (decomp.). <sup>1</sup>H-NMR (DMSO-*d*<sub>6</sub>) δ: 9.75 (1H, s), 8.30 (1H, s), 7.38 (1H, s), 6.73 (2H, dd, <sup>3</sup>J=8.00 Hz, <sup>4</sup>J=1 Hz), 6.66 (2H, dd, <sup>3</sup>J=8.00 Hz, <sup>4</sup>J=1 Hz), 3.99 (3H, s), 2.09 (3H, s), 1.86 (3H, s). IR (KBr) cm<sup>-1</sup>: 3433, 3033, 2952, 1662, 1571. MS *m/z*: 337.00 (M<sup>+</sup>+1), 231.00. *Anal.* Calcd for C<sub>18</sub>H<sub>16</sub>N<sub>4</sub>OS: C, 64.26; H, 4.79; N, 16.65. Found; C, 64.10; H, 4.55; N, 16.32.

#### *N*-(4-Chlorophenyl)pyrido[3',2':4,5]thieno[3,2-*d*]pyrimidin-4-amine (4a)

Yield 50%; mp 255–256°C. <sup>1</sup>H-NMR (DMSO-*d*<sub>6</sub>) δ: 9.39 (1H, s), 8.72 (1H, d, <sup>3</sup>J=4.5 Hz), 8.49 (1H, d, <sup>3</sup>J=8.1 Hz), 7.78 (1H, s), 7.67 (2H, d, <sup>3</sup>J=9.00 Hz), 7.37 (1H, t, <sup>3</sup>J=8.1 Hz), 7.27 (2H, d, <sup>3</sup>J=9.00 Hz). <sup>13</sup>C-NMR (DMSO-*d*<sub>6</sub>) δ: 161.62, 161.19, 157.28, 150.43, 133.95, 133.20, 131.00, 129.61, 127.98, 120.29, 118.69. IR (KBr) cm<sup>-1</sup>: 3415, 1686, 1571. MS *m/z*: 312.00 (M<sup>+</sup>), 203.00. *Anal.* Calcd for C<sub>15</sub>H<sub>9</sub>ClN<sub>4</sub>S: C, 57.60; H, 2.90; N, 17.91. Found; C, 57.32; H, 2.75; N, 17.51.

#### *N*-(4-Chlorophenyl)-7,9-dimethylpyrido[3',2':4,5]thieno[3,2-*d*]pyrimidin-4-amine (4b)

Yield 59%; mp 280–281°C. <sup>1</sup>H-NMR (DMSO-*d*<sub>6</sub>) δ: 10.89 (1H, s), 8.00 (2H, s), 7.52 (2H, d, <sup>3</sup>J=9.00 Hz), 7.09 (2H, d, <sup>3</sup>J=9.00 Hz), 2.10 (3H, s), 1.92 (3H, s). <sup>13</sup>C-NMR (DMSO-*d*<sub>6</sub>) δ: 159.98, 157.46, 152.51, 147.16, 146.57, 132.20, 124.19, 122.74, 121.28, 110.00, 24.03, 18.92. IR (KBr) cm<sup>-1</sup>: 3438, 2919, 1665, 1465. MS *m/z*: 340.00 (M<sup>+</sup>). *Anal.* Calcd for C<sub>17</sub>H<sub>13</sub>ClN<sub>4</sub>S: C, 59.91; H, 3.84; N, 16.44. Found; C, 60.30; H, 4.10; N, 16.63.

#### *N*-(2,4-Dichlorophenyl)pyrido[3',2':4,5]thieno[3,2-*d*]pyrimidin-4-amine (5a)

Yield 56%; mp > 300°C (decomp.). <sup>1</sup>H-NMR (DMSO-*d*<sub>6</sub>) δ: 9.06 (1H, s), 8.38 (1H, s), 7.71 (1H, s), 7.55 (1H, dd, <sup>3</sup>J=5.00 Hz, <sup>4</sup>J=2.00 Hz), 7.47 (1H, dd, <sup>3</sup>J=8.00 Hz, <sup>4</sup>J=2.00 Hz), 7.24 (1H, m), 6.83 (2H, m). <sup>13</sup>C-NMR (DMSO-*d*<sub>6</sub>) δ: 161.33, 150.25, 136.59, 130.92, 130.81, 130.67, 130.55, 129.11, 119.64. IR (KBr) cm<sup>-1</sup>: 1659, 1470. MS *m/z*: 345.00 (M<sup>+</sup>), 203.00. *Anal.* Calcd for C<sub>15</sub>H<sub>8</sub>Cl<sub>2</sub>N<sub>4</sub>S: C, 51.89; H, 2.32; N, 16.14. Found; C, 52.01; H, 2.54; N, 16.42.

#### *N*-(2,4-Dichlorophenyl)-7,9-dimethylpyrido[3',2':4,5]thieno[3,2-*d*]pyrimidin-4-amine (5b)

Yield 63%; mp > 300°C (decomp.). <sup>1</sup>H-NMR (DMSO-*d*<sub>6</sub>) δ: 9.49 (1H, s), 8.40 (1H, s), 7.69 (1H, s), 7.63 (1H, d, <sup>3</sup>J=9.00 Hz), 7.41 (1H, d, <sup>3</sup>J=9.00 Hz), 6.68 (1H, s), 2.89 (3H, s), 2.60 (3H, s). <sup>13</sup>C-NMR (DMSO-*d*<sub>6</sub>) δ: 161.99, 158.07, 157.28, 150.43, 144.09, 129.61, 126.00, 122.00, 118.69, 20.26, 13.87. IR (KBr) cm<sup>-1</sup>: 3301, 2905, 1692, 1574. MS *m/z*: 374.00 (M<sup>+</sup>), 231.00. *Anal.* Calcd for C<sub>17</sub>H<sub>12</sub>Cl<sub>2</sub>N<sub>4</sub>S: C, 54.41; H, 3.22; N, 14.93. Found; C, 54.79; H, 3.38; N, 15.26.

### General Procedures for the Synthesis of *N*-(Substituted Benzyl)pyrido[3',2':4,5]thieno[3,2-*d*]pyrimidin-4-amines (6–8a, b)

The appropriate benzylamine (9 mmol) was dissolved in dry DCM (25 mL) and Et<sub>3</sub>N (1.5 mL) under nitrogen atmosphere. Compound (1a or b) (4.5 mmol) was added slowly to the stirred solution which was then heated under reflux for 6–9 h. The reaction mixture was cooled and poured onto crushed ice. The precipitated solid was filtered off, washed with water (2×10 mL) and dried. The crude solid was purified by column chromatography over silica gel using 1–5 EtOAc/hexane v/v as the eluent to give the desired compounds (6–8a, b).

*N*-(Benzyl)pyrido[3',2':4,5]thieno[3,2-*d*]pyrimidin-4-amine (**6a**)

Yield 64%; mp 214–216°C. <sup>1</sup>H-NMR (DMSO-*d*<sub>6</sub>) δ: 8.36 (1H, s), 7.71 (1H, s), 7.55 (1H, d, <sup>3</sup>*J*=4.8 Hz), 7.47 (1H, d, <sup>3</sup>*J*=7.8 Hz), 7.38 (6H, m), 4.91 (2H, s). <sup>13</sup>C-NMR (DMSO-*d*<sub>6</sub>) δ: 159.59, 150.98, 147.17, 146.49, 138.40, 135.68, 131.36, 130.79, 130.56, 127.70, 122.69, 121.58, 110.60, 61.62. IR (KBr) cm<sup>-1</sup>: 3469, 2987, 1622, 1460. MS *m/z*: 292.00 (M<sup>+</sup>). *Anal.* Calcd for C<sub>16</sub>H<sub>12</sub>N<sub>4</sub>S: C, 65.73; H, 4.14; N, 19.16. Found; C, 65.51; H, 3.92; N, 18.89.

*N*-(Benzyl)-7,9-dimethylpyrido[3',2':4,5]thieno[3,2-*d*]pyrimidin-4-amine (**6b**)

Yield 71%; mp 262–263°C. <sup>1</sup>H-NMR (DMSO-*d*<sub>6</sub>) δ: 9.66 (1H, s), 8.16 (2H, s), 7.75 (5H, m), 4.31 (2H, s), 1.81 (6H, s). <sup>13</sup>C-NMR (DMSO-*d*<sub>6</sub>) δ: 160.92, 159.47, 158.33, 144.97, 126.53, 123.75, 123.27, 107.80, 61.52, 23.98, 18.05. IR (KBr) cm<sup>-1</sup>: 3467 (N-H), 3031, 2944, 1662, 1443. MS *m/z*: 320.00 (M<sup>+</sup>). *Anal.* Calcd for C<sub>18</sub>H<sub>16</sub>N<sub>4</sub>S: C, 67.47; H, 5.03; N, 17.49. Found; C, 67.19; H, 4.80; N, 17.13.

*N*-(3-Bromobenzyl)pyrido[3',2':4,5]thieno[3,2-*d*]pyrimidin-4-amine (**7a**)

Yield 57%; mp 286–288°C. <sup>1</sup>H-NMR (DMSO-*d*<sub>6</sub>) δ: 8.60 (1H, dd, <sup>3</sup>*J*=4.80 Hz, <sup>4</sup>*J*=2.00 Hz), 8.10 (1H, dd, <sup>3</sup>*J*=8 Hz, <sup>4</sup>*J*=2.00 Hz), 7.89 (1H, s), 7.64 (1H, t, <sup>3</sup>*J*=8 Hz), 7.40 (1H, s), 7.19 (3H, m), 6.48 (1H, s), 4.49 (2H, s). IR (KBr) cm<sup>-1</sup>: 3299, 2890, 1662, 1454. MS *m/z*: 369.00 (M<sup>+</sup>). *Anal.* Calcd for C<sub>16</sub>H<sub>11</sub>BrN<sub>4</sub>S: C, 51.76; H, 2.99; N, 15.09. Found; C, 52.12; H, 3.23; N, 15.31.

*N*-(3-Bromobenzyl)-7,9-dimethylpyrido[3',2':4,5]thieno[3,2-*d*]pyrimidin-4-amine (**7b**)

Yield 62%; mp 300°C. <sup>1</sup>H-NMR (DMSO-*d*<sub>6</sub>) δ: 8.91 (1H, s), 7.49 (4H, m), 6.99 (1H, s), 6.63 (1H, s), 4.39 (2H, s), 1.93 (3H, s), 1.62 (3H, s). IR (KBr) cm<sup>-1</sup>: 3433, 2963, 1662, 1455. MS *m/z*: 398.00 (M<sup>+</sup>), 231.00. *Anal.* Calcd for C<sub>18</sub>H<sub>15</sub>BrN<sub>4</sub>S: C, 54.14; H, 3.79; N, 14.03. Found; C, 53.99; H, 3.55; N, 13.79.

*N*-(3,4-Dichlorobenzyl)pyrido[3',2':4,5]thieno[3,2-*d*]pyrimidin-4-amine (**8a**)

Yield 53%; mp > 300°C (decomp.). <sup>1</sup>H-NMR (DMSO-*d*<sub>6</sub>) δ: 8.60 (1H, d, <sup>3</sup>*J*=5.00 Hz), 8.39 (1H, d, <sup>3</sup>*J*=8.00 Hz), 8.19 (1H, s), 7.41 (1H, t, <sup>3</sup>*J*=8.00 Hz), 7.31 (1H, s), 7.13 (1H, d, <sup>3</sup>*J*=9.00 Hz), 6.80 (1H, d, <sup>3</sup>*J*=9.00 Hz), 5.26 (1H, s), 3.97 (2H, s). IR (KBr) cm<sup>-1</sup>: 2983, 1696, 1464. MS *m/z*: 360.00 (M<sup>+</sup>). *Anal.* Calcd for C<sub>16</sub>H<sub>10</sub>Cl<sub>2</sub>N<sub>4</sub>S: C, 53.20; H, 2.79; N, 15.51. Found; C, 53.37; H, 2.95; N, 15.77.

*N*-(3,4-Dichlorobenzyl)-7,9-dimethylpyrido[3',2':4,5]thieno[3,2-*d*]pyrimidin-4-amine (**8b**)

Yield 59%; mp > 300°C (decomp.). <sup>1</sup>H-NMR (DMSO-*d*<sub>6</sub>) δ: 8.19 (1H, s), 7.79 (1H, d, <sup>3</sup>*J*=9.00 Hz), 7.51 (1H, s), 7.34 (1H, d, <sup>3</sup>*J*=9.00 Hz), 6.68 (1H, s), 6.16 (1H, s), 4.20 (2H, s), 2.09 (3H, s), 1.90 (3H, s). IR (KBr) cm<sup>-1</sup>: 2984, 1658, 1465 (C=N). MS *m/z*: 388.00 (M<sup>+</sup>). *Anal.* Calcd for C<sub>18</sub>H<sub>14</sub>Cl<sub>2</sub>N<sub>4</sub>S: C, 55.53; H, 3.62; N, 14.39. Found; C, 55.68; H, 3.76; N, 14.67.

**Biological Evaluation**

## Protein Kinase Inhibitory Assays

The protein kinase inhibitory assays were carried out by BPS Bioscience at single dose concentration of 10 μM.<sup>15)</sup> VEGFR-1/Flt1 (BPS #40223), VEGFR-2/KDR (BPS #40301), the wild type of EGFR (BPS #40187), CDK5/p25 (BPS #40105), GSK3α (BPS #40006), GSK3β (BPS #40007) served as enzymes sources. While GSKtide (BPS), Histone H1 (NEB #M2501S), Poly(Glu, Tyr) sodium salt, (4:1, Glu:Tyr) (Sigma

#P7244) served as the standardized substrate, in addition to kinase-GloTM Plus luminescence kinase assay kit (Promega #V3772) and ADP-GloTM kinase assay kit (Promega #V9101). The IC<sub>50</sub> determination was carried out where quality control testing was routinely performed on each of the targets to insure compliance to acceptable standards. 33P-ATP was purchased from PerkinElmer, Inc. and ADP-GloTM was purchased from Promega. All the other materials were of standard laboratory grade.

## Assay Protocols

The assays for VEGFR-2/KDR, EGFR, CDK5/p25, GSK3α and GSK3β were performed using kinase-GloTM Plus luminescence kinase assay kit (Promega #V3772). It measures kinase activity by quantitating the amount of ATP remaining in solution following a kinase reaction. The luminescent signal obtained from the assay is correlated with the amount of ATP present and is inversely correlated with the amount of kinase activity. The compounds were diluted in 10% dimethyl sulfoxide (DMSO) and 5 μL of the dilution was added to a 50 μL reaction so that the final concentration of DMSO is 1% in all of reactions. All of the enzymatic reactions were conducted at 30°C for 40 min. The 50 μL reaction mixture contains 40 mM Tris, pH 7.4, 10 mM MgCl<sub>2</sub>, 0.1 mg/mL bovine serum albumin (BSA), 1 mM dithiothreitol (DTT), 10 μM ATP, kinase substrate and the enzyme. After the enzymatic reaction, 50 μL of kinase-GloTM plus luminescence kinase assay solution (Promega #V3772) was added to each reaction and incubate the plate for 5 min at room temperature. Luminescence signal was measured using Tecan Infinite M1000 microplate reader. The assay for VEGFR-1/Flt1 was performed using ADP-GloTM kinase assay reagents (Promega #V9101). It measures kinase activity by quantitating the ADP amount produced from the enzymatic reaction. The luminescent signal from the assay is correlated with the amount of ADP present and is directly correlated with the amount of kinase activity. Other conditions were the same as the previous procedures, except the final reaction volume was reduced to 25 μL. After the 40 min kinase reaction at 30°C, 25 μL of ADP-GloTM reagent was added and incubated for 45 min at room temperature followed by another 50 min incubation with 50 μL of kinase detection mixture. Luminescence signal was measured using a Tecan Infinite M1000 microplate reader. The protein kinase assays used to determine IC<sub>50</sub> value were performed using ADP-GloTM assay kit from Promega which measures the generation of ADP by the protein kinase. Generation of ADP by the protein kinase reaction leads to an increase in luminescence signal in the presence of ADP-GloTM assay kit. The assay was started by incubating the reaction mixture in a 96-well plate at 30°C for 30 min. After the 30 min incubation period, the assay was terminated by the addition of 25 mL of ADPGloTM Reagent (Promega). The 96-well plate was shaken and then incubated for 40 min at ambient temperature, 50 mL of kinase detection reagent was added, the 96-well reaction plate was then read using the ADP-GloTM luminescences protocol on a GloMaxTM plate reader (Promega: Catalog #E7031). Blank control was set up that included all the assay components except the addition of appropriate substrate (replace with equal volume of kinase assay buffer). The corrected activity for each protein kinase target was determined by removing the blank control value.<sup>15)</sup>

### Data Analysis

Kinase activity assays were performed in duplicate at each concentration. The luminescence data was analyzed using the computer software, graph pad Prism. The difference between luminescence intensities in the absence of kinase (Lut) and in the presence of kinase (Luc) was defined as 100% activity (Lut–Luc). Using luminescence signal (Lu) in the presence of the compound, % activity was calculated as: % activity =  $[(\text{Lut}-\text{Lu})/(\text{Lut}-\text{Luc})] \times 100\%$ , where Lu = the luminescence intensity in the presence of the compound (all percent activities below zero were set to 0%). % Inhibition was calculated as: % inhibition =  $100 (\%) - \% \text{ activity}$ .<sup>15)</sup>

### Measurement of Potential Enzyme Inhibitory Activity IC<sub>50</sub>

IC<sub>50</sub> value for compound (**5a**) against EGFR was estimated by generating a graph of log inhibitor *versus* normalized response with variable using the prism software.<sup>15)</sup>

### Evaluation of Anticancer Activity against a Panel of Sixty Human Cancer Cell Lines

The structures of the final compounds were submitted to National Cancer Institute “NCI,” Bethesda, Maryland, U.S.A., and all the submitted compounds were selected on the basis of the degree of structure variation and computer modeling techniques for evaluation of their cytotoxic activity. The screening is based on the evaluation of all compounds against the full NCI 60 cell lines panel representing leukemia, non-small cell lung cancer, melanoma, colon cancer, CNS cancer, breast cancer, ovarian cancer, renal cancer and prostate cancer at a single dose of  $10^{-5}$  M. The output from the single dose screen is reported as a mean graph.<sup>21,28,29)</sup>

### Assay Protocol

The human cancer cell lines of the cancer-screening panel are grown in RPMI 1640 medium containing 5% fetal bovine serum and 2 mM L-glutamine. For a typical screening experiment, cells are inoculated into 96 well microtiter plates in 100 mL at plating densities ranging from 5000 to 40000 cells/well depending on the doubling time of individual cell lines. After cell inoculation, the microtiter plates are incubated at 37°C, 5% CO<sub>2</sub>, 95% air and 100% relative humidity for 24h prior to addition of experimental drugs. After 24h, two plates of each cell line are fixed *in situ* with trichloroacetic acid (TCA), to represent a measurement of the cell population for each cell line at the time of drug addition (Tz). Experimental drugs are solubilized in DMSO at 400-fold the desired final maximum test concentration and stored frozen prior to use. At the time of drug addition, an aliquot of frozen concentrate is thawed and diluted to twice the desired final maximum test concentration with complete medium containing 50 mg/mL gentamicin. Additional 4-, 10-fold or 1/2 log serial dilutions are made to provide a total of five drug concentrations plus control. Aliquots of 100 mL of these different drug dilutions are added to the appropriate microtiter wells already containing 100 mL of medium, resulting in the required final drug concentrations. Following drug addition, the plates are incubated for an additional 48h at 37°C, 5% CO<sub>2</sub>, 95% air, and 100% relative humidity. For adherent cells, the assay is terminated by the addition of cold TCA. Cells are fixed *in situ* by the gentle addition of 50 mL of cold 50% (w/v) TCA (final concentration, 10% TCA) and incubated for 60 min at 4°C. The supernatant is discarded, and the plates are washed five times with tap water and air dried. Sulforhodamine B (SRB) solution (100 mL) at 0.4% (w/v) in 1% acetic acid is added to

each well, and plates are incubated for 10 min at room temperature. After staining, unbound dye is removed by washing five times with 1% acetic acid and the plates are air dried. Bound stain is subsequently solubilized with 10 mM trizma base, and the absorbance is read on an automated plate reader at a wavelength of 515 nm. For suspension cells, the methodology is the same except that the assay is terminated by fixing settled cells at the bottom of the wells by gently adding 50 mL of 80% TCA (final concentration, 16% TCA).<sup>21,28,29)</sup>

### Data Analysis

Using the seven absorbance measurements [time zero, (Tz), control growth, (C), and test growth in the presence of drug at the five concentration levels (Ti)], the percentage growth is calculated at each of the drug concentrations levels. Percentage growth inhibition is calculated as:  $[(\text{Ti}-\text{Tz})/(\text{C}-\text{Tz})] \times 100$  for concentrations for which  $\text{Ti} \geq \text{Tz}$  and  $[(\text{Ti}-\text{Tz})/\text{Tz}] \times 100$  for concentrations for which  $\text{Ti} < \text{Tz}$ : three dose response parameters are calculated for each experimental agent. Growth inhibition of 50% (GI<sub>50</sub>) is calculated from  $[(\text{Ti}-\text{Tz})/(\text{C}-\text{Tz})] \times 100 = 50$  which is the drug concentration resulting in a 50% reduction in the net protein increase (as measured by SRB staining) in control cells during the drug incubation. The drug concentration resulting in total growth inhibition (TGI) is calculated from  $\text{Ti} = \text{Tz}$ . The LC<sub>50</sub> (concentration of drug resulting in a 50% reduction in the measured protein at the end of the drug treatment as compared to that at the beginning) indicating a net loss of cells following treatment is calculated from  $[(\text{Ti}-\text{Tz})/\text{Tz}] \times 100 = -50$ . Values are calculated for each of these three parameters if the level of activity is reached; however if the effect is not reached or is exceeded, the value for that parameter is expressed as greater or less than the maximum or minimum concentration tested. Results for each compound were reported as a mean graph of the percent growth of the treated cells when compared to the untreated control cells. There after obtaining the results for one dose assay, analysis of historical Development Therapeutics Program (DTP) was performed and compounds which satisfies predetermined threshold inhibition criteria is selected for NCI full panel 5 dose assay.<sup>18,28,29)</sup>

### Cytotoxicity Test

#### Cell Culture

A549 human lung cancer cells and MCF-7 human breast cancer cells were grown in RPMI-1640 medium, supplemented with 10% heat inactivated fetal bovine serum (FBS), 50 units/mL of penicillin and 50 g/mL of streptomycin and maintained at 37°C in a humidified atmosphere containing 5% CO<sub>2</sub>. The cells were maintained as “monolayer culture” by serial subculturing.<sup>27)</sup>

#### SRB Cytotoxicity Assay

The cytotoxicity was determined using SRB method as described by Skehan *et al.*<sup>27)</sup> Exponentially growing cells were collected using 0.25% Trypsin–ethylenediaminetetraacetic acid (EDTA) and seeded in 96-well plates at 1000–2000 cells/well in RPMI-1640 supplemented medium. After 24h, cells were incubated for 72h with various concentrations of the tested compounds. Following 72h treatment, the cells will be fixed with 10% trichloroacetic acid for 1h at 4°C. Wells were stained for 10min at room temperature with 0.4% SRB dissolved in 1% acetic acid. The plates were air dried for 24h and the dye was solubilized with Tris–HCl for 5min on a shaker at 1600 rpm. The optical density (OD) of each well was

measured spectrophotometrically at 564 nm with an ELISA microplate reader (ChroMate-4300, FL, U.S.A.). The  $IC_{50}$  values were calculated according to the equation for Boltzman sigmoidal concentration–response curve using the nonlinear regression fitting models (Graph Pad, Prism Version 5).<sup>27)</sup>

#### DNA-Flow Cytometry Analysis

A549 cells at a density of  $2 \times 10^5$  cells were exposed to the tested compounds at their  $IC_{50}$  concentration for 48 h. The cells were collected by trypsinization, washed in phosphate buffered saline (PBS) and then fixed in ice-cold absolute alcohol. Thereafter, cells were stained using Cycle TEST™ PLUS DNA Reagent Kit (BD Biosciences, San Jose, CA, U.S.A.) according to the manufacturer's instructions. Cell-cycle distribution was determined using a FACS Calibur flow cytometer (BD Biosciences).<sup>30)</sup>

#### Western Blot Analysis

Primary antibody against p27<sup>kip</sup> (Cell Signaling, Danvers, MA, U.S.A.) was used to assess the protein expression of this marker in the tested cells as described previously.<sup>30)</sup> Cells were seeded, cultured and exposed to the tested agent for 72 h. Whole-cell protein lysates were prepared according to standard protocol using RIPA buffer (Cell Signaling). Protein (50 mg) was loaded per well of a 10% sodium dodecyl sulfate–polyacrylamide gel electrophoresis (SDS-PAGE) gel using electrophoresis buffer (0.192 M glycine, 25 mM Tris and 0.1% SDS). After electrophoresis, the gel was transferred onto a PVDF membrane (Bio-Rad Laboratorie, Hercules, CA, U.S.A.) using transfer buffer (0.192 M glycine, 25 mM Tris, 0.025% SDS and 10% methanol). Membranes were blocked in TBS-T with 5% BSA and incubated overnight with the primary antibody (1:1000) then incubated with secondary horseradish peroxidase (HRP)-linked antibody (1:5000). Development was done using Optiplotchemiluminescent substrate (Abcamplc, Cambridge, MA, U.S.A.). Anti- $\beta$ -actin antibody (dilution, 1:5000; Abcamplc) was used to for loading correction.

Assessment of the Effect of Compounds (4b) and (5a) on P27<sup>kip</sup> Using ELISA

The effects of the tested compounds on the protein levels of P27<sup>kip</sup> were further confirmed using enzyme-linked immunosorbent assay kit from Abcamplc according to the manufacturer's instructions. Protein content of the cell lysates were assessed using BCA kit (Biovision, Inc., Milpitas, CA, U.S.A.) and the levels of P27<sup>kip</sup> were expressed as ng/mg protein of cell lysates.

#### Test for Cytotoxicity in Normal Placental Trophoblast Cells

Normal placental trophoblasts were utilized for the purpose of assessing the selective cytotoxicity of the tested agents. The villous 3A cytotrophoblast first trimester placental cell line (CRL-1584, ATCC, Manassas, VA, U.S.A.) was used. The cells were maintained in EMEM medium supplemented with 10% fetal bovine serum and 1% penicillin/streptomycin in a humidified incubator at 37°C supplemented with 5% CO<sub>2</sub>. The cells were seeded at density of  $75 \times 10^3$  cells/well in 24-well plates and incubated overnight to allow for optimum attachment. The following day, cells were exposed to the tested agents at a concentration equal to the  $IC_{50}$  against A549 cancer cells and the incubation was continued for 72 h. At the end of the exposure period the cells were stained using SRB as described previously.<sup>27)</sup> Percent viability was expressed as the relative percentage of optical density at 545 nm compared to control.

## Conclusion

EGFR is considered as a key enzyme in the regulation of cellular metabolism, growth and proliferation. Most EGFR inhibitors are discovered to date act as ATP-competitive inhibitors. Inspired by the scaffolds of the previously reported EGFR inhibitors, a novel series of pyridothieno[3,2-*d*]pyrimidin-4-amine derivatives bearing substituted anilines and benzylamines at position 4 were designed and synthesized. The rational of our study was based on the investigation of novel ATP-competitive EGFR inhibitors. The biological studies highlighted a novel EGFR inhibitor (5a) with  $IC_{50}$  value 36.7 nM. This compound showed a significant cell growth inhibition against leukemia, CNS cancer and NSCLC cell lines that overexpress EGFR, with  $GI_{50}$  values around 10 nM. The standard COMPARE analyses demonstrated a considerable correlation between compound (5a) and erlotinib with PCC value 0.727. It is worth noting that the identification of this lead compound could help in the design of clinically useful ATP-competitive EGFR inhibitors.

**Acknowledgments** The authors are grateful to The National Cancer Institute, Maryland, U.S.A. for performing the anticancer activity and also would like to thank BPS Bioscience for performing kinase inhibitory assays.

**Conflict of Interest** The authors declare no conflict of interest.

**Supplementary Materials** The online version of this article contains supplementary materials.

## References and Notes

- Mowafy S., Farag N., Abouzid K., *Eur. J. Med. Chem.*, **61**, 132–145 (2013).
- Li S., Sun X., Zhao H., Tang Y., Lan M., *Bioorg. Med. Chem. Lett.*, **22**, 4004–4009 (2012).
- Liu B., Bernard B., Wu J. H., *Proteins Structure Function and Bioinformatics*, **65**, 331–346 (2006).
- Yassen A. S. A., Elshihawy H. A. A., Said M. M. A., Abouzid K. A. M., *Chem. Pharm. Bull.*, **62**, 454–466 (2014).
- Dutta P. R., Maity A., *Cancer Lett.*, **254**, 165–177 (2007).
- Phoujdar M. S., Kathiravan M. K., Bariwal J. B., Shah A. K., Jain K. S., *Tetrahedron Lett.*, **49**, 1269–1273 (2008).
- Elsayed M. S. A., El-Araby M. E., Serya R. A. T., El-Khatib A. H., Linscheid M. W., Abouzid K. A. M., *Eur. J. Med. Chem.*, **61**, 122–131 (2013).
- Stamos J., Sliwkowski M. X., Eigenbrot C., *J. Biol. Chem.*, **277**, 46265–46272 (2002).
- Liao J. J.-L., *J. Med. Chem.*, **50**, 409–424 (2007).
- Traxler P. M., Furet P., Mett H., Buchdunger E., Meyer T., Lydon N., *J. Med. Chem.*, **39**, 2285–2292 (1996).
- Showalter H. D., Bridges A. J., Zhou H., Sercel A. D., McMichael A., Fry D. W., *J. Med. Chem.*, **42**, 5464–5474 (1999).
- Zhang J., Yang P. L., Gray N. S., *Nat. Rev. Cancer*, **9**, 28–39 (2009).
- Loidreau Y., Marchand P., Dubouilh-Benard C., Nourrisson M., Duflos M., Lozach O., Loaëc N., Meijer L., Besson T., *Eur. J. Med. Chem.*, **58**, 171–183 (2012).
- Aziz Y. M. A., Said M. M., Shihawy H. A. E., Abouzid K. A. M., *Bioorg. Chem.*, **60**, 1–12 (2015).
- <http://www.bpsbioscience.com/biochemical-based-assays>.
- This work is submitted to Academy of Scientific Research and Technology, Egyptian Patent Office, number 1468/2014.
- Erlotinib: European Medicines Agency assessment report,

- EMA/657134/2011.
- 18) <http://www.dtp.nci.nih.gov/branches/btb/ivclsp.html>.
- 19) Heimberger A. B., Learn C. A., Archer G. E., McLendon R. E., Chewing T. A., Tuck F. L., Pracyk J. B., Friedman A. H., Friedman H. S., Bigner D. D., Sampson J. H., *Clin. Cancer Res.*, **8**, 3496–3502 (2002).
- 20) Lee S. M., *Thorax*, **61**, 98–99 (2006).
- 21) <http://dtp.nci.nih.gov/docs/compare/compare.html>.
- 22) Huether A., Hopfner M., Sutter A. P., Schuppan D., Scherubl H., *J. Hepatol.*, **43**, 661–669 (2005).
- 23) Singh N., Jindal A., Behera D., *World J. Clin. Oncol.*, **5**, 858–864 (2014).
- 24) Pestell R. G., Albanese C., Reutens A. T., Segall J. E., Lee R. J., Arnold A., *Endocr. Rev.*, **20**, 501–534 (1999).
- 25) Chu I. M., Hengst L., Slingerland J. M., *Nat. Rev. Cancer*, **8**, 253–267 (2008).
- 26) Fang Y., Wang Y., Wang Y., Meng Y., Zhu J., Jin H., Li J., Zhang D., Yu Y., Wu X. R., Huang C., *Biochem. J.*, **463**, 383–392 (2014).
- 27) Skehan P., Storeng R., Scudiero D., Monks A., McMahon J., Vistica D., Warren J., Bokesch H., Kenney S., Boyd M. R., *J. Natl. Cancer Inst.*, **82**, 1107–1112 (1990).
- 28) Alley M. C., Scudiero D. A., Monks A., Hursey M. L., Czerwinski M. J., Fine D. L., Abbott B. J., Mayo J. G., Shoemaker R. H., Boyd M. R., *Cancer Res.*, **48**, 589–601 (1988).
- 29) Grever M. R., Schepartz S. A., Chabner B. A., *Semin. Oncol.*, **19**, 622–638 (1992).
- 30) Tolba M. F., Esmat A., Al-Abd A. M., Azab S. S., Khalifa A. E., Mosli H. A., Abdel-Rahman S. Z., Abdel-Naim A. B., *IUBMB Life*, **65**, 716–729 (2013).